

Intrabody Communication for Implants in Body Area Network Scenarios

Assefa K. TESHOME^{a,1}, Behailu KIBRET^a and Daniel T. H. LAI^a

^aCollege of Engineering and Science, Victoria University Melbourne

Abstract. This paper studies implant communication in the Wireless Body Area Networks (WBAN) and presents a novel analytical electromagnetic model for galvanically coupled Intra-body Communication (IBC) for implants. The model is versatile to be applied to any part of the human body as it is based on multilayered ellipsoidal geometry. Experimental validation and Finite Difference Time Domain (FDTD) analysis show that the model is highly accurate for implant-to-implant and implant-to-surface communication. With high degree of miniaturizability, path loss at the surface of the skin is found to around 35 dB; that shows Galvanically coupled IBC implants are a good alternative compared to existing wireless implants.

Keywords. Intra-body Communication, Implants, Galvanically Coupled IBC.

1. Introduction

To improve accuracy and timeliness of diagnosis, electronic devices could be implanted inside human body to provide various real-time diagnostics information. However, effective technique for implant communication is still an open problem. Currently, in accordance with Medical Implant Communication Services (MICS) standard, radio-frequency (RF) implant wireless communication is enabled by utilizing small antennas that radiate radio waves inside the human body in the 402–405 MHz frequency range. In fact, MICS was later adopted as Medical Devices Radiocommunications Services (MedRadio) for 401–406 MHz frequency range [1].

As a bid to find alternative wireless implant communication model within the Wireless Body Area Network (WBAN), in this work, the authors explored galvanically coupled IBC for implant-to-surface communication. IBC is a relatively new technique that uses the human body as a channel with communication frequencies not exceeding several MHz. Specifically, this paper examines a new analytical electromagnetic model that uses galvanically coupled IBC where the implant transmitter differentially injects current into the tissue via its anode and cathode electrodes. A wearable receiver on the surface of the skin samples the resulting potential difference using its two electrodes. Frequencies ranging from hundreds of kHz up to a few MHz are considered under quasi static assumptions. The model is unified in the sense that it is based on multilayered ellipsoidal geometry that can be applied to any part of the body (i.e., head, torso, limbs etc.). It also effectively describes influences of tissue layer thicknesses and electromagnetic proper-

¹Corresponding Author: Assefa K. Teshome, Victoria University; E-mail: assefa.teshome@live.vu.edu.au.

ties, implant size and depth, and geometry of the body part. The security and low power consumption of IBC are also apparent in this model. The path loss characterisation of IBC implants shows lower values compared to their MICS counterparts.

The remainder of this paper is organised as follows: Section 2 discusses implant communication in WBAN scenario. Section 3 motivates the framework of our model setup where analytical expression for electric potential distribution is derived by treating special functions called Lamé's functions in an ellipsoidal coordinate system. Section 4 discusses the effect of tissue layers on potential distribution and path loss. Section 5 presents experimental validation of the analytical model and our conclusion is given in Section 6.

2. Implant Communication in the WBAN Architecture

The general architecture of body area sensor networks, as shown in Fig. 1(a), is that a link node wearable on the surface talks to and listens from the implanted and other surface mounted devices. It then combines and relays the signal to devices external to the body – mainly a monitoring or controlling device away from the body. Another likely scenario is the possibility of two implants talking to each other; for example, a glucose sensor and an insulin pump. To reduce complexity and power consumption it is better to implement advanced security features at the link node rather than each individual implanted or on-body device. To avoid eavesdropping attempts to listen or talk to sensors in and on the body by any transceiver external to the body, the signal needs to be confined to within the body. For frequencies ranging from a few hundreds of kHz to tens of MHz, the human body hardly radiates radio waves. Thus, this band is suitable for body confined (intra-body) transmissions – implant-to-implant, implant-to-surface and surface-to-surface. To communicate the signal to outside the body wirelessly, radio wave propagation of RF signals is required. Such is the case for the link node or possibly an individual implant is desired to directly communicate with the outside environment. For this scenario, our previous works [2, 3] explored using the human body as an antenna in the frequency ranging from 10–110 MHz. Furthermore, the human body resonance frequency is found to be between 30–70 MHz which falls within the frequency of interest.

For implant communication it is important that the transmitter consumes small power to conserve battery life. The implant should also be miniaturized for a minimal invasive embedding. Besides, due to sensitive nature of medical data, security is a paramount requirement of implant communication. To achieve security either the signal needs to be encrypted at the transmitter or be confined to within the body detectable by as far as an on-body receiver. In the case of MICS based implant, the signal is radiated outside the human body; hence, requires all security features be implemented right at the transmitter which increases the transmitter complexity. Hence, the transmitter consumes large power and is difficult to miniaturise. Thus, due to the fact that the signal is confined to within the body, galvanically coupled IBC implants promise a larger degree of miniaturisation compared to their MICS counterparts.

3. The Human Body as a Channel for Implant Communication (HBC)

The HBC uses an electric field communication (EFC) where the human body is effectively a volume conductor. It exploits the lossy dielectric nature of the conductive tissue

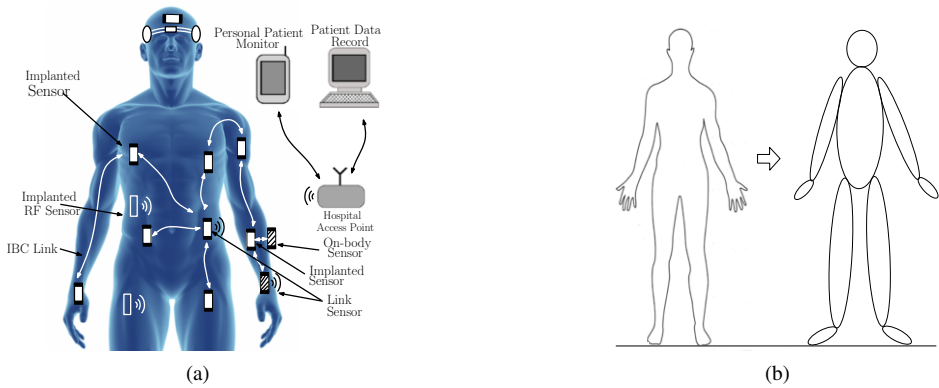


Figure 1. (a) IBC in the WBAN architecture. (b) Ellipsoidal approximation of parts of the human body.

layers to induce a current, and hence a potential distribution, as a result of the electric field caused by the current injected by the transmitter electrode(s). Such a low frequency signal is expected to penetrate deeper into the tissue layers, thus requiring less power be detected by a receiver on the surface of skin. Moreover, due to a non-conducting free space outside the skin surface, the signal is confined to within the human body.

3.1. Galvanically Coupled IBC Model for Implant Communication

In literature, several modelling techniques have been used to model the human body as a channel. Some of these techniques include the circuit models [4–6] and electromagnetic propagation models [7–11]. Each model shows various useful aspects of intra-body communication. However, the electromagnetic models used are based on simple geometries which limit their use to only specific regions of the body. On the other hand, circuit models are generally short-sighted in the sense that the relationship between channel variations and circuit components is not obvious in the transfer functions, albeit well characterized channels in fixed settings.

The analytical electromagnetic model presented on this paper is motivated by geometries robust enough to capture tissue layer effects in a scalable way that can be applied to any part of the body and yet simple enough to guarantee analytical solutions. Based on this geometry, a mathematical model of the channel is derived to characterise the received signal as a function of the size of the transmitter, tissue layers of the body part, transmitter location, receiver location and electrode spacing.

Most body parts can be approximated by a variation of the ellipsoidal geometry as shown in Fig. 1(b). For example, the human head can be modeled using an ellipsoid close to spherical symmetry. The torso can be modeled by a prolate or oblate spheroid versions of the ellipsoidal geometry. Limbs can be modelled by an ellipsoid where a dominating semi-axis represents the limb length whereas the other two axes represent the larger and the shorter radii of the limb. When one of the semi-axes is large and the other two are comparable, the geometry resembles a cylinder which is often used in existing electromagnetic models e.g. [9, 11]. Hence, analytical model based on multilayered ellipsoidal representation of tissue layers can represent the various body parts by defining the semi-axes lengths. The ellipsoidal shells in the layers represent each tissue layer with varying thickness and complex permittivity.

3.2. Volume Conduction Theory for Implant Communication

Volume conduction can be defined as a transmission technique for electric field inside the volume of a lossy dielectric where an electric field is induced by a primary current source; and this field propagates to the receiver by means of an induction current induced in the conductive medium [12]. An implant transmitter coupled galvanically can be envisaged as the primary current source inside one or more lossy layers of body tissue. The total current inside the volume creates an electric potential distribution inside and on the surface of the volume [13]. The receiver could be either another implant or on-body device where its two electrodes are used to sample the potential difference between the two points of the body the electrodes are connected to. The transmission frequencies we consider are smaller than the high frequency band of the spectrum. From the conductivity and permittivity profiles of human body tissues at these small frequencies, electromagnetic signals in the body can be assumed to be quasi-static [9], [14]. Thus, variations of electric and magnetic fields, denoted as \mathbf{E} and \mathbf{B} respectively, with time are negligible. Hence, the set of Maxwell's equation describing the fields can be modified as follows:

$$\nabla \times \mathbf{E} = 0, \nabla \times \mathbf{B} = \mu \mathbf{J}, \nabla \cdot \mathbf{E} = 0, \nabla \cdot \mathbf{B} = 0, \tag{1}$$

where μ is permeability of free space and \mathbf{J} is the net current density inside the volume. Here, the electric field \mathbf{E} is $\mathbf{E} = -\nabla V$, where V is the electric potential distribution. The current inside the volume is due to the conduction source current density $J^s(r) = \mathfrak{M}\delta(r - r_0)$ and the induced current density $J^i(r) = \sigma(r)\mathbf{E}(r)$ where $\sigma(r)$ is the conductivity of the tissue layer at point r and \mathfrak{M} is the electric dipole moment and r_0 is the point in space that is mid-way between the transmitter electrodes. Thus, the net current density $J(r)$ is given as

$$J(r) = \mathfrak{M}\delta(r - r_0) + \sigma(r)\mathbf{E}(r). \tag{2}$$

No current flows out of the human body due to the non-conducting medium (air) outside the body; hence, is a divergent free current density (i.e., $\nabla \cdot J(r) = 0$). Taking the divergence on both sides of (2), we have

$$\nabla \cdot \sigma(r)\nabla V(r) = \nabla \cdot \mathfrak{M}\delta(r - r_0). \tag{3}$$

Equation (3) is the governing equation for the electric potential which takes different forms for the parts of the volume; i.e., it takes the form of a Poisson's equation in the region (layer) that contains the source and takes the form of a Laplace's equation in the layers that do not contain the source.

3.3. Potential Distribution: an Example Scenario

In this section the solution for the potential V in equation (4) is presented for an example scenario shown in Fig. 2. The scenario considered is the case where a transmitter is implanted inside the muscle tissue of the human arm and the receiver is placed on the surface of the skin. In this case four tissue layers are considered; i.e., bone, muscle, fat and skin. The tissue layers are represented by multi-layered confocal ellipsoidal shells. The appropriate coordinate system to solve for the potential is the Ellipsoidal coordinate

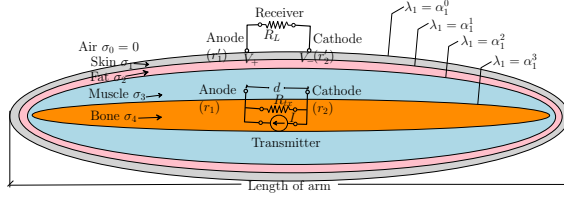


Figure 2. Longitudinal cross-section of multilayered ellipsoidal model of human arm.

system. The solution of (4) in Ellipsoidal coordinate systems can be simplified by using special functions called Lamé’s functions of the first and second kind as shown in [15]. The general form of the potential distribution inside the *i*th layer is given by

$$V_i(\lambda_1, \lambda_2, \lambda_3) = \sum_{n=0}^{\infty} \sum_{p=1}^{2n+1} A_{(n,p)}^i \mathbb{E}_n^p(\lambda_1, \lambda_2, \lambda_3) + \sum_{n=0}^{\infty} \sum_{p=1}^{2n+1} B_{(n,p)}^i \mathbb{F}_n^p(\lambda_1, \lambda_2, \lambda_3), \quad (4)$$

where λ_1, λ_2 and λ_3 are the ellipsoidal coordinate system, and are the Lamé’s function of first and second kind, respectively, with degree *p* and order *n*. $A_{(n,p)}^i$ and $B_{(n,p)}^i$ are the coefficients corresponding to the *i*th tissue layer and α_i^j is the dominating semi-axis length of the *i*th tissue layer. Equation (4) is the general solution and specific solution for every scenario is provided by thoroughly specifying the coefficients $A_{(n,p)}^i$ and $B_{(n,p)}^i$ by applying Dirichlet and Numan boundary conditions at each layer. Here for the setting given in Fig. 2, the coefficients are calculated as

$$\begin{aligned} A_{(n,p)}^0 &= 0, & B_{(n,p)}^0 &= \frac{B_{(n,p)}^1}{C_{(n,p)}^0 I_n^p(\alpha_1^0)}, \\ A_{(n,p)}^1 &= (2n+1) \left[\frac{1}{C_{(n,p)}^0} - I_n^p(\alpha_1^0) \right] B_{(n,p)}^1, & B_{(n,p)}^1 &= \frac{B_{(n,p)}^3}{\left[\left(1 - \frac{\sigma_2}{\sigma_3}\right) Q_n^p C_{(n,p)}^2 + \frac{W_n^p}{\sigma_3} \right]}, \\ A_{(n,p)}^2 &= (2n+1) \left[\frac{1}{C_{(n,p)}^0} + I_n^p(\alpha_1^1, \alpha_1^0) \right. \\ &\quad \left. - \frac{W_n^p I_n^p(\alpha_1^1)}{\sigma_2} \right] B_{(n,p)}^1, & B_{(n,p)}^2 &= \frac{W_n^p B_{(n,p)}^1}{\sigma_2}, \\ A_{(n,p)}^3 &= (2n+1) \left[Q_n^p B_{(n,p)}^1 - I_n^p(\alpha_1^2) B_{(n,p)}^3 \right], & B_{(n,p)}^3 &= \frac{\mathfrak{M} \cdot \nabla_{\mathbf{r}_0} \mathbb{E}_n^p(\lambda_{10}, \lambda_{20}, \lambda_{30})}{(2n+1) \sigma_3 \gamma_n^p}, \\ A_{(n,p)}^4 &= (2n+1) \left[Q_n^p B_{(n,p)}^1 + I_n^p(\alpha_1^3, \alpha_1^2) B_{(n,p)}^3 \right. \\ &\quad \left. - I_n^p(\alpha_1^3) B_{(n,p)}^4 \right] & B_{(n,p)}^4 &= \left(1 - \frac{\sigma_3}{\sigma_4}\right) C_{(n,p)}^3 \left[Q_n^p B_{(n,p)}^1 \right. \\ & & &\quad \left. + I_n^p(\alpha_1^3, \alpha_1^2) B_{(n,p)}^3 \right] + \frac{\sigma_3}{\sigma_4} B_{(n,p)}^4. \end{aligned} \quad (5)$$

Here, $I_n^p(\alpha_1^i, \alpha_1^j) = I_n^p(\alpha_1^i) - I_n^p(\alpha_1^j), \forall i, j \in \{0, 1, 2, 3\}$, $W_n^p = (\sigma_2 - \sigma_1) C_{(n,p)}^1 \left[\frac{1}{C_{(n,p)}^0} + I_n^p(\alpha_1^1, \alpha_1^0) \right] - \sigma_1$, and $Q_n^p = \left[\frac{1}{C_{(n,p)}^0} + I_n^p(\alpha_1^1, \alpha_1^0) + \frac{W_n^p I_n^p(\alpha_1^2, \alpha_1^1)}{\sigma_2} \right] B_{(n,p)}^1$. This completes the derivation of the potential distribution at any point within the arm. The potential difference V_{Rx} sensed at the receiver is then given by the difference of the potentials at the receiver electrode locations as $V_{Rx} = V(r'_1) - V(r'_2)$.

4. Discussion: Path Loss and Potential Distribution

To calculate the potential distribution and hence the path loss human arm model given in Fig. 2 and equations (4) and (5) are used. An arm of smallest semi-axis 43.5 mm is considered with tissue thicknesses of skin = 1.5 mm, fat = 8.5 mm, muscle = 27.5 mm, bone = 6 mm.

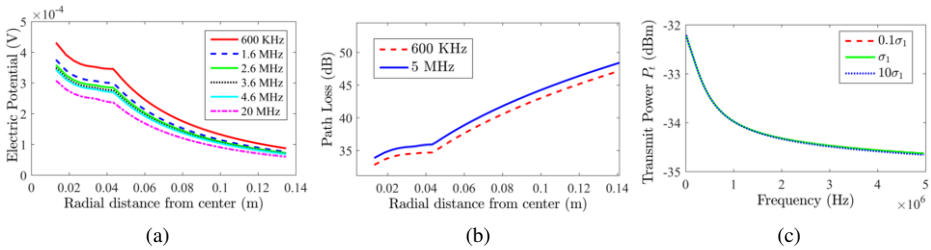


Figure 3. (a) Potential distribution with distance at different frequencies. (b) Path loss as function of distance at different frequencies. (c) Transmitted power as a function of frequency for different skin conductivity.

Consider the transmitter injecting an r.m.s. current of 1 mA with its electrodes spaced by 5 mm located along the major semi-axis of the arm at 6.9 mm into the muscle tissue from the muscle-bone interface. The maximum electric potential developed along the axis of the dipole as a function of radial distance from the center is shown in Fig. 3(a). The received potential decreases at a slower rate inside the body and decreases at a faster rate once the signal leaves the body. This can also be seen in the path loss which increases at a large slope outside the skin as shown in Fig 3(b). The path loss at the surface of the skin is around 35 dB which is a lot smaller than the path loss reported for MICS based implants. The impedance of the tissue layer affects the amount of power transmitted. From Fig. 3(c) the transmit power decreases with frequency which due to decreasing impedance with frequency. The transmitted power is around -32 to -35 dBm; hence, the received power is around -67 dBm to -70 dBm. The received power is thus larger than the average receiver sensitivity of -92.5 dBm required by IEEE 802.15.6 standard.

5. Model Validation

In our experimental validation, path loss measurements were conducted by transmitting signals through a phantom solution that is prepared to mimic conductivity and permittivity of muscle tissue at 13.56 MHz. The phantom solution is prepared according to the recipe given by Haggmann *et al* [16]. The aqueous solution is poured into a container shown in Fig. 4(a) with dimensions $h = 12\text{cm}$, $b = 9\text{cm}$ and $w = 34\text{cm}$ (the container roughly resembles a human arm).

A pair of shielded BNC cables is connected to the transmitter and receiver copper electrodes as shown in Fig. 4(a). Both the transmitter and receiver electrodes are prepared with 3 cm electrode spacing. A Vector Network Analyzer (VNA) is used to analyze the channel between the transmitter and receiver. The VNA we used is the Pro miniVNA (miniVNA Pro, Mini Radio Solutions Inc., Poland). The transmitter and receiver electrodes are connected, respectively, to the DUT and DET ports of the VNA via a 50 Ohm

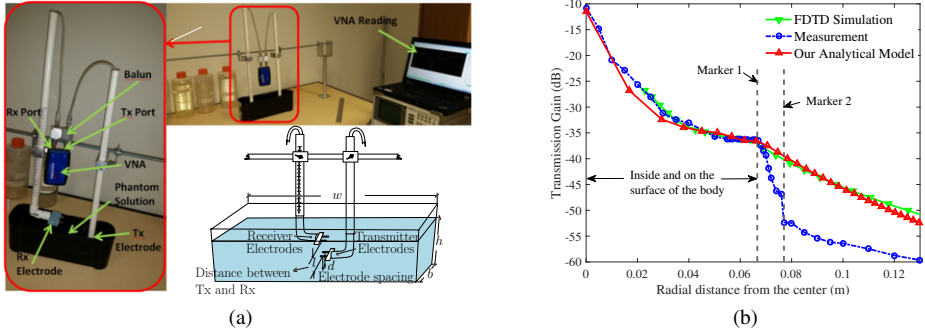


Figure 4. (a) Experimental setup for validation of proposed model. (b) Comparison of our model with measurement and simulation.

Balun. Vertically, the transmitter is submerged at a depth of 6.7cm from the outer surface of the phantom solution. Horizontally, both the transmitter and receiver electrodes are located at the center of the 34 cm long phantom solution. The vertical position of the receiver electrodes is varied and path loss readings were recorded in a Laptop wirelessly connected to the VNA via BlueTooth.

We have also conducted FDTD simulation using SMECADx software for the same setting. The receiver can either be another implant or mounted on the surface of the skin. Thus, our region of interest (ROI) is the region inside and on the surface of the body. For this region, up to 6.7 cm radial distance from the center (i.e., marker 1 in Fig. 4(b), our analytical model and the FDTD simulation fit the measurement reasonably well as shown in Fig. 4(b). However, as we leave the surface of the skin, the measured path loss is larger than predicted by our model and the FDTD simulation, although the trend is similar after marker 2. According to [17], we believe the discrepancy outside the body is mainly due to the electrode contact impedance which is not considered in our model and the FDTD simulation. Inside the body, the receiver electrodes are connected and surrounded by a conducting tissue where both the conduction and induced currents exist; hence, the contact established is similar to metal-to-electrolyte contact and its effect to the path loss is negligible [18, 19]. Outside the body, the electrodes measure a high impedance which can not be ignored. This contact impedance increases as the electrodes move away from a conducting body. Hence, the measured path loss increases at a larger gradient than modeled between vertical marker 1 and maker 2 as shown in in Fig. 4(b). After some distance far enough for the conducting tissues to least affect the electrode contacts, the contact impedance does not change considerably. Thus, after marker 2, the measured path loss roughly takes slower slope as predicted by the FDTD and our model. The fact that contact impedance is large outside the body further strengthens the claim that IBC signal is confined to within the body.

6. Conclusion

In this paper, we presented a novel analytical model of galvanically coupled IBC for implant communication. The model is geometrically versatile to be used in any part of human body. Thus, our model can be to analytically study the electromagnetic effect of

tissue layers, size and depth of the implant, path loss and received potential. Our experimental validation results align reasonably well with the model in the ROI. The model indicates that galvanically coupled implant communication is not only feasible but possesses a better path loss characteristics and a potentially large degree of miniaturisation.

References

- [1] S. Hanna, "Regulations and standards for wireless medical applications," in *Proceedings of the 3rd international symposium on medical information and communication technology*, 2009, pp. 23–26.
- [2] B. Kibret, A. K. Teshome, and D. T. Lai, "Characterizing the human body as a monopole antenna," *IEEE Transactions on Antennas and Propagation*, vol. 63, no. 10, pp. 4384–4392, 2015.
- [3] —, "Analysis of the human body as an antenna for wireless implant communication," *IEEE Transactions on Antennas and Propagation*, vol. 64, no. 7, 2016.
- [4] W. Besio and A. Prasad, "Analysis of skin-electrode impedance using concentric ring electrode," in *EMBS'06. 28th Annual International Conference of the IEEE*. IEEE, 2006, pp. 6414–6417.
- [5] K. Hachisuka, Y. Terauchi, Y. Kishi, K. Sasaki, T. Hirota, H. Hosaka, K. Fujii, M. Takahashi, and K. Ito, "Simplified circuit modeling and fabrication of intrabody communication devices," *Sensors and actuators A: physical*, vol. 130, pp. 322–330, 2006.
- [6] B. Kibret, M. Seyedi, D. T. H. Lai, and M. Faulkner, "Investigation of galvanic-coupled intrabody communication using the human body circuit model," in *IEEE J. Biomed. Health Inform.*, vol. 18, no. 4, July 2014, pp. 1196–1206.
- [7] J. A. Ruiz, J. Xu, and S. Shimamoto, "Propagation characteristics of intra-body communications for body area networks," in *3rd IEEE CCNC 2006.*, vol. 1. IEEE, 2006, pp. 509–513.
- [8] J. Bae, H. Cho, K. Song, H. Lee, and H.-J. Yoo, "The signal transmission mechanism on the surface of human body for body channel communication," in *IEEE Trans. Microw. Theory Techn.*, vol. 60, no. 3, March 2012, pp. 582–593.
- [9] S. H. Pun, Y. M. Gao, P. Mak, M. Vai, M. Du *et al.*, "Quasi-static modeling of human limb for intrabody communications with experiments," *Information Technology in Biomedicine, IEEE Transactions on*, vol. 15, no. 6, pp. 870–876, 2011.
- [10] M. S. Wegmueller, S. Huclova, J. Froehlich, M. Oberle, N. Felber, N. Kuster, and W. Fichtner, "Galvanic coupling enabling wireless implant communications," *IEEE Trans. Instrum. Meas.*, vol. 58, no. 8, pp. 2618–2625, 2009.
- [11] M. Amparo Callejon, J. Reina-Tosina, D. Naranjo-Hernández, and L. M. Roa, "Galvanic coupling transmission in intrabody communication: A finite element approach," *IEEE Trans. Biomed. Eng.*, vol. 61, no. 3, pp. 775–783, 2014.
- [12] C. E. Tenke and J. Kayser, "Generator localization by current source density (CSD): implications of volume conduction and field closure at intracranial and scalp resolutions," *Clinical neurophysiology*, vol. 123, no. 12, pp. 2328–2345, 2012.
- [13] S. B. Rutkove, "Introduction to volume conduction," *The clinical neurophysiology primer*, vol. 388, p. 43, 2007.
- [14] R. Plonsey and D. B. Heppner, "Considerations of quasi-stationarity in electrophysiological systems," *The Bulletin of mathematical biophysics*, vol. 29, no. 4, pp. 657–664, 1967.
- [15] A. K. Teshome, B. Kibret, and D. T. Lai, "Galvanically coupled intra-body communications for medical implants: A unified analytic model," *IEEE Transactions on Antennas and Propagation*, DOI:10.1109/TAP.2016.2559519, vol. 64, no. 7, 2016.
- [16] M. Haggmann, R. Levin, L. Calloway, A. Osborn, and K. Foster, "Muscle equivalent phantom materials for 10-100 MHz," *IEEE Trans. on Microwave Theory and Tech.*, vol. 40, no. 4, pp. 760–762, 1992.
- [17] A. Hördt, P. Weidelt, and A. Przyklenk, "Contact impedance of grounded and capacitive electrodes," *Geophysical Journal International*, vol. 193, no. 1, pp. 187–196, 2013.
- [18] L. Geddes and R. Roeder, "Criteria for the selection of materials for implanted electrodes," *Annals of biomedical engineering*, vol. 31, no. 7, pp. 879–890, 2003.
- [19] I. A. Hokajärvi, "Electrode contact impedance and biopotential signal quality," *Thesis, Tampere University of Technology, Finland*, 2012.